Vitamin D deficiency increases prostatic megalin expression and globulin-bound testosterone import, increasing prostatic androgens in African American men

Jason Garcia[1], Kirstin D. Krieger[1], Candice Loitz[1], Lillian Perez[1,2], Zachary A. Richards[1], Yves Helou[1], Steve Kregel[1], Clementina A. Mesaros[4,5], Peter H. Gann[1,2], Donald Vander Griend[1,2], Rick Kittles[6], Gail S. Prins[1,2,7], Trevor Penning[4,5], Larisa Nonn[1,2,*]

[1]Department of Pathology, University of Illinois at Chicago, Chicago, IL 60612, USA
[2]University of Illinois Cancer Center, Chicago, IL 60612, USA
[3]Mass Spectrometry, Metabolomics and Proteomics Facility, University of Illinois at Chicago, Chicago, IL 60612, USA
[4]Department of Systems Pharmacology & Translational Therapeutics, University of Pennsylvania Perelman School of Medicine, Philadelphia, PA 19104, USA
[5]Center of Excellence in Environmental Toxicology, Perelman School of Medicine, University of Pennsylvania, Philadelphia, PA 19104, USA
[6]Department of Population Sciences, City of Hope, Duarte, CA 91010, USA
[7]Departments of Urology, Physiology and Biophysics, University of Illinois at Chicago, Chicago, IL 60612, USA

Correspondence: Larisa Nonn, PhD
Professor of Pathology
840 S. Wood St.
Chicago, IL 60612
312-996-0194
lnonn@uic.edu

Keywords: vitamin D, androgen, prostate cancer, disparities

ABSTRACT

Vitamin D deficiency associates with an increased risk of prostate cancer (PCa) mortality and is hypothesized to contribute to PCa aggressiveness and disparities in African Americans. We reported a relationship between African-ancestry, circulating and intraprostatic vitamin D metabolites and prostatic expression of megalin, an endocytic membrane receptor that internalizes globulin-bound hormones. Here, we show that megalin imports sex hormone-binding globulin (SHBG)-bound testosterone, potentially regulating intraprostatic hormone levels. Vitamin D levels regulated megalin expression in cell lines, patient-derived prostate epithelial cells, and prostate tissue explants, and mice with prostatic knockout of *Lrp2* (megalin) showed reduced prostatic testosterone. Notably, prostatic 5α-dihydrotestosterone levels were higher in African American men and correlated inversely with serum vitamin D status, while megalin protein levels were reduced in PCa tissue. Our findings highlight the negative impact of vitamin D deficiency on PCa and the potential link to PCa disparities observed in African Americans.

INTRODUCTION

Prostate cancer (PCa) is the second most frequently diagnosed cancer in men in the United States, and African American (AA) men have 60% higher incidence and 200% higher mortality rates than European American (EA) men [1]. The reason for this disparity is multifactorial and involves biological and socioeconomic factors; yet, when controlled for, AA men still present with more aggressive disease [2]. AA men are also at increased risk for deficiencies in vitamin D, a steroid hormone essential for normal human physiology and calcium homeostasis [3]. Vitamin D status is dependent on supplementation, sun exposure, and skin pigmentation; melanin reduces cutaneous vitamin D synthesis [4]. Vitamin D metabolites exert anti-transformative properties in PCa cells and delay the formation of preneoplastic lesions in a mouse model of PCa [5]. Importantly, circulating levels of the prohormone 25D are inversely correlated with aggressive PCa [6-11]. Thus, disparities in vitamin D are hypothesized to underlie this disparity in PCa in AA men, but the mechanistic pathways remain unclear.

Further, while serum 25D levels are used to assess vitamin D status clinically and in epidemiologic studies, local tissue concentrations of vitamin D metabolites are understudied [12]. Only a small percentage of vitamin D metabolites exist free in circulation, and the majority (88–99%) are bound by vitamin D-binding protein (DBP) or albumin [13]. The free hormone hypothesis suggests that intracellular concentrations of vitamin D metabolites and other hormones are dependent on passive diffusion of hormones not bound by serum globulins [14]. However, we demonstrated that circulating levels of the hormonally active vitamin D metabolite 1,25-dihydroxyvitamin D (1,25D) and prostatic levels of 1,25D do not correlate, indicating that passive diffusion of unbound hormone is not driving 1,25D in the prostate [15]. Because nearly all serum vitamin D metabolites are bound by DBP, our data support a mechanism by which these bound metabolites are actively imported into the prostate.

One candidate that may support an active import mechanism is megalin, an endocytic receptor encoded by *LRP2* with a well-characterized function of binding and internalizing DBP-bound 25D from the glomerular filtrate [16,17]. We confirmed that prostate epithelium expresses megalin protein and discovered that prostatic expression of *LRP2* negatively correlates with 25D levels only in AA men and positively correlates with percent West African ancestry. These findings suggest that the free hormone hypothesis may not apply in the prostate, and that an ancestry-specific compensatory mechanism may increase vitamin D transport into prostate epithelium when systemic levels are deficient.

Megalin also binds and internalizes sex hormone-binding globulin (SHBG), the serum transporter of testosterone (T). Megalin import of SHBG-bound T occurs in kidney cells [18], and import of SHBG occurs in LNCaP cells [19]. Circulating T concentrations do not correlate with intraprostatic concentrations, further supporting an alternative to passive diffusion [20]. Notably, megalin-deficient mice exhibit defects in maturation of their reproductive organs [18], suggesting dysregulation of sex hormones.

We hypothesize that megalin plays a role in an ancestry-specific, compensatory mechanism to increase prostatic import of androgen and vitamin D metabolites. This mechanism is highly relevant to PCa disparities since androgens contribute to PCa pathogenesis [21]. Here, we performed a mechanistic examination of steroid hormone transport by megalin in prostate cells, patient prostate tissue explants from AA patients and mouse model. We further examine hormone and megalin levels in clinical specimens.

RESULTS

Prostate cells express megalin and import SHBG-bound T

Megalin transcript (*LRP2*) and protein expression was compared between prostate cells and HEK-293 kidney cells (positive control). Both gene and protein were detected in benign primary patient-derived prostate epithelial cells (PrE AA1 and PrE AA2), immortalized benign prostate epithelial cells (957E-hTERT), and in PCa cell lines (LAPC-4, 22Rv1) (**Figure 1A,B**). Whereas benign PrE cells lack androgen receptor (AR) expression, LAPC-4 and 22Rv1 PCa cell lines express AR and SRD5A1, catalyzers of T to DHT, and were therefore used to examine androgen import (T) and AR activity in vitro. When treated with T alone and SHBG-T, both LAPC-4 and 22Rv1 cells showed AR activation, as evidenced by increased *KLK3* mRNA and an AR-driven luciferase construct containing two androgen response elements (AREs) from the probasin promoter (ARR2PB) (**Figure 1C,D**). SHBG was added at 20-fold excess and incubated with T for 30 min before treating cells to ensure thorough globulin binding. To demonstrate that the response to SHBG-T involves megalin, cells were preincubated with receptor-associated protein, a megalin inhibitor (MEG-Inh) (**Figure 1C,D**) [22]. Both LAPC-4 and 22Rv1 cells exhibited decreased *KLK3* gene expression and ARE luciferase when cells were pretreated with MEG-Inh before hormone treatments; however, the magnitude of inhibition was higher in 22Rv1 cells, which express more megalin. Preincubation with MEG-Inh did not block the response of added T alone (**Figure S1**). To visualize SHBG-T internalization, we used Alexa Fluor 555-labeled SHBG (SHBG-555). SHBG-555 localized to the plasma membrane of LAPC-4 and 22Rv1 cells in response to SHBG and SHBG + T treatment (**Figure 1E**). Addition of SHBG-T showed more internalization and punctate patterns than SHBG treatment alone, and MEG-Inh blocked the internalization of SHBG. These data demonstrate that SHBG-bound T is available to prostate cells in a megalin-dependent manner.

Knockout of *Lrp2* in mouse prostate reduces T

To determine if prostate T levels are affected by the absence of megalin, we created a prostate-specific knockout of *Lrp2* since full *Lrp2* knockout is perinatal lethal [23]. Tamoxifen (TAM)-inducible prostate-specific knockout of *Lrp2* was generated by crossing an *Lrp2*-floxed mouse [24] (a gift from Dr. Willnow) with the probasin-driven TAM-inducible Cre recombinase mouse (Pb-MerCreMer) [25] (**Figure 2A**). We encountered no breeding problems with the homozygous bitransgenic line. $Lrp2^{fl/fl}/cre^{+/+}$ mice and control ($Lrp2^{fl/fl}$ only and $cre^{+/+}$ only) mice were injected with TAM at postnatal day 10 (P10-TAM), which resulted in recombination of DNA in only the prostate and not in mouse tails (**Figure 2B**). Day 10 injections were stopped due to complications with injecting young pups, and subsequent injections were at 5 weeks. Prostates, testes, and sera were collected at 24 and 32 weeks of age for androgen measurement by liquid chromatography–tandem mass spectrometry (LC–MS/MS). There were no significant differences prostate hormones between P10-TAM and 5W-TAM animals. Prostate T and DHT levels were significantly lower in $Lrp2^{fl/fl}/cre^{+/+}$ mice than in control mice, (**Figure 2C**). Serum T and testes T levels were tightly correlated in all mice, supporting testes as the source of serum T. However, neither prostate T nor DHT significantly correlated to serum T in control and $Lrp2^{fl/fl}/cre^{+/+}$ mice (**Figure 2D**), suggesting that prostate T levels are not due to passive diffusion from the serum. Also, prostate T and DHT only significantly correlated in the control $Lrp2^{fl/fl}$ only, suggesting regulation of T to DHT is different in the prostates lacking *lrp2*. Serum DHT was undetectable in most mice. Although the differences in androgens were significant, there were no differences in prostate histology, prostate weight, and fertility (data not shown). Relationships between serum and tissue hormone levels support a regulated transport mechanism of T into the prostate, rather than passive diffusion of serum T.

Vitamin D and androgen negatively regulate *LRP2* expression

Our previous study found a negative correlation between serum vitamin D metabolites and *LRP2* expression in AA men [15], suggesting negative regulation of *LRP2* by vitamin D. Therefore, we sought to characterize the impact of vitamin D on *LRP2* expression in vitro. Primary prostate epithelial cells (PrE-AA1) treated with 10 nM 25D exhibited decreased *LRP2* expression (**Figure 3A**). Because our results showed that SHBG-T was imported into PCa cells (**Figure 1**), we also examined regulation of *LRP2* by T and observed a similar suppressive effect (**Figure 3A**).

To assess the regulation of *LRP2* expression at the transcriptional level, we characterized *LRP2* promoter activity in vitro. The *LRP2* promoter was cloned into a *Renilla* luciferase reporter plasmid (*LRP2-Rluc*), which was suppressed in 957E-hTERT cells by 25D and in 22Rv1 cells by T (**Figure 3B**; **Figure S2**). 957E-hTERT cells are advantageous for luciferase experiments because they can be transfected at a high efficiency. Further, 957E-hTERT cells are benign epithelial prostate cells that do not express AR and are similar to PrE cells in phenotype. The vitamin D receptor (VDR) forms an obligate heterodimer with retinoid X receptor (RXR) and binds to vitamin D response elements (VDREs). Analysis of this *LRP2* promoter fragment [26] identified multiple RXR:VDR and AR motifs (**Figure 3C**; **Figure S2**). These transcriptional analyses support the hypothesis that *LRP2* expression is regulated by hormone-stimulated transcription factors in response to 25D and T.

PrE and 957E cells respond to 25D but do not express AR. Conversely, 22rV1 cells do not have active CYP27B1 to bioactivate 25D. Thus, we examined these responses in fresh ex vivo benign human prostate tissue slice cultures (**Figure 3D**), which express all components of androgen and vitamin D activation/response pathways, including *CYP27B1* (vitamin D 25-hydroxylase), *VDR*, *LRP2*, and *SRD5A* (T to DHT conversion), and *AR* (data not shown). Hormone responsiveness was demonstrated by robust induction of *CYP24A1* and *KLK3* gene expression by 25D and T, respectively, alone or in the presence of their serum-binding

globulins, DBP and SHBG (**Figure 3E**)**.** Megalin protein and *LRP2* expression were decreased in tissue slices treated with 25D alone or T (**Figures 3F,G**), consistent with our observation in cell lines and the relationships observed in patient data [15]. Examination of murine prostate epithelial *Lrp2* gene expression in publicly available single-cell RNA-sequencing data showed upregulation after castration and downregulation following regeneration with T (**Figure S3**). These findings strongly support vitamin D-mediated negative-feedback on *LRP2* expression and identify a second feedback loop regulated by androgens.

Intraprostatic DHT is higher in AA men and inversely correlates with vitamin D status

Data showing that *LRP2* expression is negatively regulated by 25D and that globulin-bound T is able to enter prostate cells and tissues suggest that vitamin D deficiency may lead to megalin upregulation and, subsequently, increased import of steroid hormones. To test this hypothesis, we examined the relationships between these hormones in patients. We quantified T and DHT in serum and in benign areas of radical prostatectomy tissue from a cohort of patients with PCa patients for whom we had previously measured vitamin D metabolites [15]. Vitamin D status, as measured by serum 25D level, negatively correlated with intraprostatic DHT (**Figure 4A**). AA patients had higher prostate levels of the active hormones 1,25D and DHT (**Figure 4B**) and lower levels of serum T (**Figure 4C**) than EA men. This relationship is consistent with our report on vitamin D metabolites in AA men [15], identifying 25D as lower in the serum but 1,25D as higher in prostate. The serum and tissue levels of vitamin D metabolites shown here are a subset of the full cohort reported by us in 2017 [15]. Prostate T levels were undetectable in the majority of patients (**Figure 4D**), supporting metabolism to DHT once in the tissue. A few patients had high prostatic T with low DHT, suggesting that they may have been on 5α-reductase inhibitors at the time of surgery. Finally, serum DHT levels were lower than serum T (**Figure 4D**) and did not differ by ancestry. Overall, the inverse correlation of serum

25D with intraprostatic DHT supports our hypothesis that serum vitamin D deficiency and low serum T are drivers of higher prostatic DHT levels.

Megalin and *LRP2* levels fluctuate during PCa progression

A tissue microarray (TMA) composed of prostate cores from 29 patients (20 AA, 9 EA) with four cores from each patient, two benign and two PCa regions per patient, was stained for megalin. Fluorescence intensity was digitally quantified in epithelial regions using the epithelial marker Pan-CK to segment the epithelium (**Figure 5A**). Frozen tissues were not available for patients represented in this TMA; therefore, we could not correlate tissue hormone levels with megalin expression. Megalin protein levels were significantly lower in PCa areas than in benign tissues in the overall cohort (P = 0.02) and to a similar degree in AA (P = 0.0006) and EA subgroups, although the difference in EA men was not significant due to small sample size (**Figure 5B**). To examine megalin in metastatic PCa, we analyzed *LRP2* mRNA expression in an RNA-sequencing cohort composed of 25 localized tumors and 32 metastatic prostate tumors [27-29]. *LRP2* mRNA expression was higher in metastatic sites than in the localized tumor (**Figure 5C**).

DISCUSSION

This study follows our recent finding that megalin protein is expressed in the membrane of prostate epithelium and that megalin gene expression correlates with vitamin D status and percentage of African ancestry [15]. These findings led us to hypothesize that megalin is part of a compensatory pathway to increase intraprostatic vitamin D metabolites when patients are deficient [15]. Here, we show that megalin imports SHBG-bound T, is regulated by T and vitamin D, and is dysregulated in PCa. These findings provide a direct link between vitamin D deficiency and the disparity of PCa in AA men.

Seventy percent of circulating T is bound to SHBG [19] with about 5% free T and the remaining bound to albumin. T is thought to follow the free hormone hypothesis, with only free or albumin-bound T available to tissues. We show that megalin binds and internalizes SHBG-bound T, which is similar to other reports in LNCaP cells [19]. This occurred in PCa cell lines and fresh prostate tissue slices, which internalized SHBG-bound T resulting in *KLK3* induction. We further demonstrated that loss of megalin in mouse prostate epithelium decreased prostate levels of androgens. Although knockout mice demonstrate some regulation of prostate T by megalin, it is important to note that adult male mice primarily circulate albumin-bound T rather than SHBG-T. However, megalin is multiliganded and also mediates albumin uptake [30]. Our findings do not rule out the presence of other SHBG-T uptake receptors [31]. The data shown here support megalin-dependent import of SHBG-T into the prostate and are consistent with full *Lrp2* knockout, which displays impaired descent of the testes into the scrotum and other defects consistent with sex steroid disruption [18].

A negative feedback loop was reported for vitamin D skeletal myotube cultures in which growth in high levels of 25D significantly decreased DBP-bound 25D uptake in cultures [32]. We similarly observed that high levels of 25D decreased the expression of *LRP2* and megalin protein. T also negatively regulated megalin, demonstrating interplay between hormones, likely to tightly control the intracellular levels of steroids. This was also observed *in vivo* in mouse prostates following castration and regeneration with exogenous androgens.

The presence of a compensatory feedback loop to regulate intraprostatic hormones levels has implications for the AA population who are disproportionately vitamin D deficient [33]. In our cohort, serum 25D and prostatic DHT were significantly inversely correlated, consistent with vitamin D regulation of hormone import via megalin. Moreover, AA men had higher levels of DHT in prostate tissue than EA men and lower levels of serum T, further supporting active transport of SHBG-T rather than passive diffusion of T. The tight correlation of prostate and

serum levels of vitamin D metabolites and androgen metabolites suggests coregulation. Further, elevated prostatic DHT may directly contribute to the increased incidence of aggressive PCa and PCa mortality among AA men. This relationship outlines an intricate yet detrimental interaction between androgen and vitamin D axes that characterizes the adverse effects of a double disparity in men of West African descent.

Our serum finding that serum T is higher in AA men differs from prior studies that found no racial differences in serum total T or free T [34,35]. This discrepancy may reflect differential assay and sample preservation methods . Although our results were significant, we acknowledge that there is a limitation of underrepresentation of vitamin D-replete AA patients and vitamin D-deficient EA patients in the cohort, which is needed to separate ancestry from deficiency.

Given the dependence of PCa on androgens, we examined megalin protein and *LRP2* gene expression in multiple cohorts of PCa patients. Megalin protein was markedly lower in cancer tissue than in benign tissue in radical prostatectomy samples. In contrast to our findings in localized PCa, *LRP2* expression was increased in metastatic disease, which may be an attempt to increase tumor T levels in response to low hormone concentration in the metastatic site. Altogether, these data may characterize a dual role for megalin during PCa progression. Megalin expression may be a phenotype of differentiated epithelium; thus, the decrease in localized PCa is a result of the loss of differentiation in the tumor. However, megalin expression may increase in metastases to increase the tumor's access to SHBG-bound T.

The interplay between vitamin D status, megalin, and cancer may also extend to breast cancer, another hormone-responsive disease. For example, HME-immortalized breast epithelial cells and T47D breast cancer cells are able to internalize DBP-bound 25(OH)D and activate *CYP24A1* [36]. Additional work shows that SHBG binds circulating estradiol and, as of 2016, AA women are nearly 1.5 times more likely to develop lethal triple-negative breast cancer than

white women [37]. These studies show that megalin-mediated endocytosis of globulin-bound hormones extends to breast tissue and could perhaps outline a double disparity that contributes to increased breast cancer mortality in AA women.

An important consideration regarding race-related differences is that race is a social construct and a proxy for ancestry. We are not suggesting that there are biological differences by a patient's self-declared race. Rather, because vitamin D status is directly correlated to skin pigmentation, our findings suggest that vitamin D supplementation may reduce the levels of prostate androgens, which would mostly affect AA men who tend to be vitamin D deficient.

In conclusion, our in vitro and ex vivo data show that megalin is functional in the prostate and responsible for transporting protein-bound hormones into the cell, which complicates the free hormone hypothesis. We also show that megalin expression is negatively regulated by vitamin D, and, in times of deficiency, megalin is upregulated, potentially increasing import of both vitamin D and T. This may signify a once-protective compensatory mechanism of vitamin D gone awry, increasing the likelihood of androgen import and increasing the probability of harmful androgen actions that may contribute to the disparity in PCa aggressiveness that plagues AA men.

METHODS

Cell lines

HEK293, LAPC-4, and 22Rv1 cells were purchased from ATCC (VA, USA), and 957E-hTERT cells were generously donated by John Isaacs and maintained in keratinocyte serum-free medium (KSFM) (ThermoFisher Scientific). PrE-AA1 and PrE-AA2 cells are primary patient-derived epithelial cells derived in our lab by previously reported methods [38,39]. HEK293 cells were maintained in Dulbecco's Modified Eagle's medium (DMEM) (Gibco) supplemented with 10% (vol/vol) fetal bovine serum (FBS) (Gibco). LAPC-4 and 22Rv1 cells were maintained in phenol-free Roswell Park Memorial Institute (RPMI) (Gibco) medium supplemented with 10%

(vol/vol) FBS. Cells were switched to 5% (vol/vol) charcoal-stripped FBS (Millipore-Sigma) overnight and serum starved for 1 h before experimentation. Primary prostate cells established from fresh male radical prostatectomy tissues were isolated as previously described [38,39] and cultured in prostate cell growth medium (Lonza). All cells were cultured at 37°C with 5% CO_2. Enzalutamide-resistant CWR-R1 (CWR-R1-ENZR) and VCaP (VCaP-ENZR) cells were previously generated by continuous culture in RPMI and DMEM, respectively, with 10% (vol/vol) FBS and 10 μM enzalutamide for at least 6 months before experimentation [40]. All cells are described in **Table S1**.

RNA isolation and reverse transcription–quantitative PCR (RT–qPCR)

RNA was isolated by the Trizol method (ThermoFisher Scientific). RNA concentration and quality were determined by measuring the absorbance ratio at 260/280 nm using a NanoDrop One spectrophotometer (ThermoFisher Scientific). Total RNA (500 ng) was reverse transcribed using the high-cCapacity cDNA reverse transcription kit (Applied Biosystems). Resulting cDNA was used for quantitative PCR amplification on a QuantStudio6 machine (ThermoFisher Scientific) using gene-specific primers (**Table S2**) and FastStart Universal SYBR Green master mix (Millipore-Sigma). Reactions were run in duplicate, and relative C_t values were normalized and calculated independently using the $-\Delta\Delta C_t$ method [41] to the expression of the housekeeping genes *HPRT1* and *RPL13A* (all primers are listed in **Table S1**).

Western blotting

Cells were grown to 80% confluency, and protein lysates were collected in cell lysis buffer (9803, Cell Signaling Technology). Protein (30 μg) was run on a Bis-Tris protein gel (NuPAGE) and transferred to a PVDF membrane. Membranes were blocked for 1 h using Odyssey Blocking Buffer (LiCOR) and probed with anti-megalin rabbit monoclonal antibody (1:1,000;

M02463, Boster Bio) and anti-actin (1:1,000; 4499S, Cell Signaling Technology) and with secondary antibodies against rabbit and mouse (926-68071, LiCOR). Blots were imaged using the Odyssey CLx imaging system (LiCOR).

T and SHBG treatments

LAPC-4 and 22Rv1 cells at 80% confluency were incubated with 25 nM T ± 125 nM human SHBG (SHBG-8259H, Creative BioMart) and 1 μM receptor-associated protein (MEG-Inh) (BML-SE552-0100, Enzo Life Sciences) for 16 h. T and SHBG were preincubated for 30 min before addition to cells. Cells were pretreated with megalin inhibitor for 1 h before hormone addition.

Luciferase reporter assays

Cells at 70% confluency were transfected with luciferase plasmids, and luciferase activity was measured after 48 h using the dual-luciferase reporter assay system and GloMax 20/20 (Promega). For AR activity, 0.2 ng/μL ARR2PB-luciferase was used, which is a firefly luciferase that is regulated by two AREs from the probasin promoter. pRL-null *Renilla* plasmid was cotransfected at 0.4 pg/μL to control for transfection efficiency. For *LRP2* promoter, 0.2 ng/μL *LRP2* promoter-driven *Renilla* luciferase reporter (S712992, Switchgear Genomics) and 0.4 pg/μL PGL4.50 *Photinus pyralis* (E310, Promega) luciferase reporter were simultaneously treated with 10 nM 25D or 10 nM T. *Renilla* luciferase relative light units are defined as the ratio of *Renilla* to *Photinus* activity.

DBP-488 and SHBG-555 internalization

Alexa Fluor protein conjugation kits (ThermoFisher Scientific) were used to conjugate 555 reactive dye to SHBG according to the manufacturer-supplied protocol. Aliquots of globulin conjugates were stored at −20°C until use. Cells were grown to 70% confluency in eight-well

chamber slides and incubated with SHBG alone, SHBG-T, or MEG-Inh + SHBG-T as described above. After 4 h, cells were counterstained with Alexa Fluor 647 Phalloidin (F-actin) and DAPI (ThermoFisher Scientific) and visualized by confocal microscopy.

Lrp2-flox/Pb-MerCreMer mice

The University of Illinois at Chicago Office of Animal Care and Institutional Biosafety (OACIB) approved all procedures involving animals in this study. Transgenic mice harboring the probasin promoter driving MerCreMer were acquired from The Jackson Laboratory (ProbasinBAC-MerCreMer or C57BL/6-Tg(Pbsn-cre/Esr1*)14Abch/J, strain 020287) [25]. Mice with *loxP* sites flanking *Lrp2* exons 71 through 75 (*Lrp2*$^{fl/fl}$) were generously gifted by Dr. Thomas Willnow [24]. *Lrp2*$^{fl/fl}$ mice were crossbred with Pb-MerCreMer homozygous (*cre*$^{+/+}$) mice. F1 cross progeny were mated to generate *Lrp2*$^{fl/fl}$/*cre*$^{+/+}$ mice. Mice were genotyped by Transnetyx and injected with TAM (50 mg/kg) at two stages of development (P10 or 5 weeks). Control TAM-injected mice were *Lrp2*$^{fl/fl}$ or *cre*$^{+/+}$. To confirm recombination, DNA was isolated from tail snips and prostate cell pellets using a DNeasy Blood & Tissue kit (Qiagen) followed by PCR with DreamTaq Green PCR master mix (ThermoFisher Scientific) using primers spanning exons 71–75 and primers spanning exons 76–77 as a control. PCR products were imaged on agarose gels. All mouse primers are listed in **Table S2**.

Mouse DHT and T quantitation

A protocol similar to that described by Higashi et al. was followed [42]. Briefly, the internal standard mix (500 pg each of T-IS, DHT-IS, E1-IS, and E2-IS and 100 pg of 3α- and 3β-diol) were added to 0.6 mL of 0.1 mM PBS in a homogenization vial kept in ice. Frozen tissue (around 20 mg of tissue) was cut on a tile in dry ice with a blade kept in dry ice and added directly to the homogenization vial. The tissue was homogenized two times for 10 min in ice in a

Bullet Blender. The homogenate was moved to a borosilicate tube, and ethyl ether (4 mL) was added and shaken for 30 min, followed by incubation for 2 h at 50°C with shaking at 4°C overnight. The sample was then centrifuged at 1,500*g* for 10 min. Using a glass pipette, the upper organic phase was transferred into a new borosilicate tube. The organic phase was dried under nitrogen. Samples were stored at −20°C before derivatization and LC–MS analysis, as previously described [43].

Ex vivo prostate tissue slice culture

Prostate tissue from a 5-mm punch was sliced into 300-µm sections using an Alabama Tissue Slicer (Alabama Research and Development), placed on titanium alloy inserts within a six-well plate, and maintained in 2.5 mL of KSFM supplemented with 5% (vol/vol) charcoal-stripped FBS and 50 nM R1881 (PerkinElmer) [44]. Slices were cultured overnight, rotating at a 30° angle at 37°C with 5% CO_2. Alternate slices were collected for RNA extraction and formalin fixation. For gene expression, RNA isolation and RT–qPCR was performed as described above. Only slices with confirmed benign epithelial content (high expression of KRT8 and undetectable *PCA3* by RT–qPCR) were included in the analyses.

Immunohistochemistry

Formalin-fixed paraffin-embedded slices were sectioned to 5 µm, deparaffinized, processed for steam antigen retrieval (10 mM sodium citrate, 0.05% Tween 20, pH 6), and stained with anti-megalin (1:500; ab76969, Abcam) overnight at 4°C. A rabbit secondary antibody HRP/DAB kit was used to visualize with hematoxylin counterstain (ab64261, Abcam)

Patient sera and prostate tissue

Fresh-frozen prostate and sera were collected from radical prostatectomy patients. Specimens from 60 patients were included for analysis: 30 from the UIC Hospital (Chicago, Illinois, USA) and 30 from the Cooperative Human Tissue Network (CHTN) Western Division at Vanderbilt University (Nashville, Tennessee, USA). Criteria for inclusion were self-declared race data, >500 mg of benign frozen prostatectomy specimen, and availability of sera. All patients had localized PCa without prior chemotherapy or hormone therapy. Samples were obtained from two deidentified biorepositories: CHTN and UIC. Because samples were deidentified, the research was determined to not fit the definition of human subjects research by the UIC IRB (2013-0341).

Hormone measurement in patient samples

Calibration curve

Standard compounds T and DHT and internal standard (IS) d3T were purchased from Cerilliant (Round Rock, TX, USA). Nine calibrators (0.0625, 0.125, 0.25, 0.5, 1, 5, 10, 50, and 100 ng/mL in methanol) were used to establish calibration curves with spiked-in IS. Curves were fitted by linear regression with a weighting factor of 1/*x*.

Sample preparation and extraction

Tissue samples and ISs were mixed and bead homogenized using a Mikro-Dismembrator II (Handelskontor Freitag, Germany) before extraction. The extraction took place three times with hexane:ethyl acetate (60:40 [vol:vol]). The organic layer from each extraction was collected, combined, and dried under nitrogen. The residue was reconstituted in methanol:water (20:80 [vol:vol]) and subjected to solid-phase extraction using an ISOLUTE C18 SPE cartridge (100 mg, 1 mL) following the manufacturer's protocol. The final eluate was dried before for LC–MS analysis. Human serum samples were extracted by the same procedure.

LC–MS/MS analysis

Quantification of T and DHT was achieved using an SCIEX Qtrap 6500 spectrometer coupled with an Agilent 1290 ultra performance liquid chromatography (UPLC) system. Dried sample was reconstituted in methanol and resolved by a Waters ACQUITY UPLC BEH C18 column (1.7 µm, 2.1 × 100 mm) maintained at 45° at a flow rate of 450 µL/min. Elution started with 60% of mobile phase A (5% methanol in water, 0.1% formic acid), followed by a linear gradient increase of mobile phase B (acetonitrile with 0.1% formic acid) from 40 to 80%. MS data were acquired by multiple reaction monitoring (MRM) in positive mode with an electrospray ionization (ESI) source voltage at 5.0 kV and temperature at 450°C. T, DHT, and D3T were detected by monitoring their transitions to signature product ions 289>97 (T), 291>255 (DHT), and 292>97 (D3T), respectively. Data were analyzed using Analyst software.

Vitamin D metabolite measurement

Extraction and measurement of 25D was performed as previously reported by our group [15].

TMA immunostaining and analysis

The TMA contained 118 prostate biopsy cores from 29 patients (20 AA, 9 EA) and consisted of at least two benign and cancer cores from each patient. A board-certified pathologist reviewed each core to confirm cancer grade mark regions for exclusion if they contained artifacts or benign areas intermixed with cancer. Sections (5 µm) were incubated with rabbit polyclonal anti-megalin (ab76969) diluted 1:100 and mouse monoclonal anti-panCK (AE1/AE3) diluted 1:2,000, followed by incubation with secondary antibody Alexa Fluor 488 goat anti-rabbit diluted 1:200 and Alexa Fluor 555 goat anti-mouse diluted 1:200 (Life Technologies, Carlsbad, CA, USA) and counterstaining with DAPI. Sections were scanned at ×20 on a Vectra3 multispectral imaging system (Akoya Biosciences, Marlborough, MA). Epithelial areas were identified and segmented by machine learning using the panCK marker and HALO software (Indica Labs, Albuquerque,

NM) and adjusted manually to ensure accuracy. Epithelial megalin fluorescence intensity was quantified and reported as average intensity per pixel of the segmented area of each core using Inform software. A Mann–Whitney unpaired U test was used to compare benign cores to PCa cores for all men, EA only, and AA only.

LRP2 expression in public datasets

PCa tumor and metastases RNA-sequencing datasets were previously reported and described by our group [27]. *LRP2* expression was analyzed by analysis of variance (ANOVA) with Kruskal–Wallis for multiple comparisons. Mouse prostate single-cell RNA sequencing was from Karthaus et al. using data from the epithelial cluster from three mice per timepoint intact, 1, 7, and 28 days after castration, and 1, 7, and 28 days after adding back T to regenerate the prostate [45]. *Lrp2* expression was extracted from the Broad Single Cell Portal.

Statistics

Statistical analysis methods used in each experiment are detailed within the figure legends and methods.

Data availability

All data generated or analyzed during this study are included in this published article (and its supplementary information files).

DECLARATION OF INTEREST

There is no conflict of interest that could be perceived as prejudicing the impartiality of the research reported.

AUTHOR CONTRIBUTIONS

J.G., K.D.K., C.L., L.P., Z.A.R. and S.K. conducted the experiments. Y.H. maintained the mouse colony. C.A.M. conducted hormone quantitation. P.H.G. and D.V.G. provided essential patient datasets and edited the manuscript. G.S.P, R.K., T.P., and L.N. secured funding. J.G., L.P., and L.N. wrote the manuscript.

FUNDING

This research was funded by the Department of Defense Prostate Cancer Research Program Idea Award for Disparities Research PC170484 (L.N., T.P., R.K., and G.S.P.) and NIH awards 1R21CA231610-01 (L.N.) and P30-ES013508 (C.A.M. and T.P.).

ACKNOWLEDGEMENTS

Tissue samples were provided by the UI Health Biorepository and the CHTN, an NCI-supported resource. *Lrp2*-flox mice were a gift from Thomas Willnow. We thank Klara Valyi-Nagy and Alexandru Cristian Susma from the UI Health Biorepository, Ryan Deaton and the UIC research Histology and Tissue Imaging Core for assistance with the tissue microarray analysis, Vicky Macias and Andre Kajdacsy-Balla for assessment of pathology of patient tissues, Morgan Zenner and Michael Schlicht for assistance with generating tissues slices, and Hui Chen for editing the methods. Finally, we thank the patient participants and Drs. Michael Abern, Daniel Moreira, and Simone Crivellaro for procurement of radical prostatectomy tissue specimens.

FIGURE LEGENDS

Figure 1. Prostate cells express megalin and import SHBG-bound T. (A, B) Expression of *LRP2* and megalin protein in a panel of prostate cell lines as shown by RT–qPCR (A) and immunoblotting (B). RT–qPCR data are shown as relative quantitation to *HPRT*. Error bars are standard error of the mean (SEM). (C) Regulation of *KLK3* (prostate-specific antigen [PSA] gene) expression after 24 h following treatment with vehicle control (CTL), 50 nM T alone (T), 50 nM T preincubated with 500 nM SHBG (SHBG), or T + SHBG in cells preincubated with 1μM MEG-Inh in LAPC4 and 22Rv1 PCa lines. (D) Regulation of ARE luciferase activity in LAPC4 and 22Rv1 cells. Data are normalized to control Renilla activity. (E) Visualization (×63) of SHBG-555 (red) import into cells with DAPI (blue) nuclear and F-actin (green) cytoskeletal counterstains. Statistical analysis was performed using a one-way ANOVA with a two-stage linear step-up procedure of Benjamini, Krieger, and Yekutieli for multiple comparisons; **P* < 0.05 for comparison to CTL, ^*P* < 0.05 for comparison to T + SHBG. All graphs represent mean ± SEM of three or more individual experiments with two replicates per experiment.

Figure 2. Loss of *Lrp2* in mouse prostate reduces prostatic androgens. (A) Mouse model for conditional knockout of *Lrp2* in prostate epithelium. (B) Recombination of *Lrp2* exons 71–75 after TAM treatment in prostate DNA (P) but not in tail DNA (T) only in bitransgenic mice. PCR for exons 76–77 was performed as a positive control. (C) prostate levels of T and DHT quantified by LC–MS/MS for $Lrp2^{fl/fl}$ and $Lrp2^{fl/fl}/cre^{+/+}$. Graphs show mean with maximum–minimum bars. (D) Heat map of Pearson correlation coefficients (*R*) for tissue and serum androgens for P10-TAM mice ($Lrp2^{fl/fl}$ n=5, $Lrp2^{fl/fl}/cre^{+/+}$n=6). The *P* value is shown within each cell; NS, not significant.

Figure 3. Negative regulation of *LRP2* and megalin protein by vitamin D and T in cells and tissue slice explants. (A) *LRP2* expression following 24 h of treatment with 50 nM 25D or T in

PrE-AA1 or 22Rv1 cells, respectively. (B) Activity of a custom *LRP2* promoter luciferase construct after 24 h of 50 nM 25D or T treatment; RLU, relative luciferase units normalized to transfection control. (C) *LRP2* promoter contains RXR:VDR- and AR-binding motifs. (D) Ex vivo prostate tissue slice workflow. (E) Slices respond to 25D and T as shown by RT–qPCR for *CYP24A1* and *KLK3*, respectively. Sixteen hours after treatment with 50 nM 25D in the presence and absence of 0.02 μg/μL DBP or 50 nM T in the presence and absence of 250 nM SHBG. (F) Megalin protein expression by IHC in tissue slices after 24 h of treatment with 50 nM 25D or T. Scale bar = 150 μm. The graph shows the mean pathologist score per gland. (G) RT–qPCR analysis of *LRP2* expression in prostate tissue slices after 16 h of treatment with 50 nM 25D or T. Relative gene expression is shown as relative quantity (RQ) normalized to *RPL13A*; CTL, vehicle control for all experiments. For cell lines, graphs represent mean ± SEM from triplicate repeats. For tissue slices, graphs show representative experiment mean ± standard deviation (SD) with two replicates per experiment. *P* values were determined using an unpaired *t* test (A, B, and F) or by Kruskal–Wallis and Dunn's multiple comparison tests to CTL (E and G); $*P < 0.01$.

Figure 4. Ancestry-specific differences in androgen levels and relationships between DHT and 25D. (A) Correlation between serum 25D and prostate DHT in EA ($n = 29$) and AA ($n = 28$) men measured by uHPLC-MS-MS. Correlation values (r) were determined using Spearman's rank test. (B, C) Prostate tissue levels of 1,25D and DHT (B) and serum 25D and T levels measured by uHPLC-MS-MS (C). Graphs represent mean with 95% confidence interval (95% CI). The *P* values were determined by unpaired two-tailed *t* test. (D) Waterfall plots of the distribution of prostate tissue and serum androgens across the cohort (EA, $n = 29$; AA, $n = 28$)

Figure 5. Megalin expression is dysregulated in cancer. (A) Digital quantitation of epithelial megalin expression on a TMA consisting of 118 prostate biopsy cores from 29 patients (EA, $n =$

9; AA, *n* = 20). Epithelial regions were segmented by panCK staining, and benign and cancer regions were determined by a board-certified pathologist. Scale bar = 100 μm. (B) Immunofluorescence (IF) intensity per pixel for megalin expressed as mean ± SEM; Ben, benign. (C) *LRP2* expression in primary tumors and metastases (Mets) in an RNA-sequencing dataset [27]. Graphs show mean $\log_2$ fragments per kilobase of transcript per million mapped reads (FKPM) ± 95% CI. *P* values were determined by a Mann–Whitney test; ***P* < 0.001.

REFERENCES

1 Siegel, R. L., Miller, K. D. & Jemal, A. Cancer statistics, 2018. *CA Cancer J Clin* **68**, 7-30, doi:10.3322/caac.21442 (2018).

2 Rebbeck, T. R. Prostate Cancer Disparities by Race and Ethnicity: From Nucleotide to Neighborhood. *Cold Spring Harb Perspect Med* **8**, doi:10.1101/cshperspect.a030387 (2018).

3 Abern, M. R. *et al.* Race is associated with discontinuation of active surveillance of low-risk prostate cancer: results from the Duke Prostate Center. *Prostate Cancer Prostatic Dis* **16**, 85-90, doi:10.1038/pcan.2012.38 (2013).

4 Matsuoka, L. Y., Wortsman, J., Haddad, J. G., Kolm, P. & Hollis, B. W. Racial pigmentation and the cutaneous synthesis of vitamin D. *Archives of dermatology* **127**, 536-538 (1991).

5 Banach-Petrosky, W. *et al.* Vitamin D inhibits the formation of prostatic intraepithelial neoplasia in Nkx3.1;Pten mutant mice. *Clinical cancer research : an official journal of the American Association for Cancer Research* **12**, 5895-5901, doi:10.1158/1078-0432.CCR-06-1039 (2006).

6 Steck, S. E. *et al.* Association between Plasma 25-Hydroxyvitamin D, Ancestry and Aggressive Prostate Cancer among African Americans and European Americans in PCaP. *PLoS One* **10**, e0125151, doi:10.1371/journal.pone.0125151 (2015).

7 Shui, I. M. *et al.* Circulating vitamin D, vitamin D-related genetic variation, and risk of fatal prostate cancer in the National Cancer Institute Breast and Prostate Cancer Cohort Consortium. *Cancer* **121**, 1949-1956, doi:10.1002/cncr.29320 (2015).

8 Nyame, Y. A. *et al.* Associations Between Serum Vitamin D and Adverse Pathology in Men Undergoing Radical Prostatectomy. *J Clin Oncol* **34**, 1345-1349, doi:10.1200/JCO.2015.65.1463 (2016).

9 Murphy, A. B. *et al.* Vitamin D deficiency predicts prostate biopsy outcomes. *Clin Cancer Res* **20**, 2289-2299, doi:10.1158/1078-0432.CCR-13-3085 (2014).

10 Feldman, D., Krishnan, A. V., Swami, S., Giovannucci, E. & Feldman, B. J. The role of vitamin D in reducing cancer risk and progression. *Nat Rev Cancer* **14**, 342-357, doi:10.1038/nrc3691 (2014).

11 Christakos, S., Dhawan, P., Verstuyf, A., Verlinden, L. & Carmeliet, G. Vitamin D: Metabolism, Molecular Mechanism of Action, and Pleiotropic Effects. *Physiol Rev* **96**, 365-408, doi:10.1152/physrev.00014.2015 (2016).

12 Chun, R. F. *et al.* Vitamin D and DBP: the free hormone hypothesis revisited. *The Journal of steroid biochemistry and molecular biology* **144 Pt A**, 132-137, doi:10.1016/j.jsbmb.2013.09.012 (2014).

13 Cooke, N. E. & Haddad, J. G. Vitamin D binding protein (Gc-globulin). *Endocr Rev* **10**, 294-307, doi:10.1210/edrv-10-3-294 (1989).

14 Mendel, C. M. The free hormone hypothesis: a physiologically based mathematical model. *Endocr Rev* **10**, 232-274, doi:10.1210/edrv-10-3-232 (1989).

15 Richards, Z. *et al.* Prostatic compensation of the vitamin D axis in African American men. *JCI insight* **2**, e91054-e91054, doi:10.1172/jci.insight.91054 (2017).

16 Christensen, E. I., Birn, H., Storm, T., Weyer, K. & Nielsen, R. Endocytic receptors in the renal proximal tubule. *Physiology (Bethesda)* **27**, 223-236, doi:10.1152/physiol.00022.2012 (2012).

17 Nykjaer, A. *et al.* An endocytic pathway essential for renal uptake and activation of the steroid 25-(OH) vitamin D3. *Cell* **96**, 507-515 (1999).

18 Hammes, A. *et al.* Role of endocytosis in cellular uptake of sex steroids. *Cell* **122**, 751-762, doi:10.1016/j.cell.2005.06.032 (2005).

19 Li, H. *et al.* Sex Hormone Binding Globulin Modifies Testosterone Action and Metabolism in Prostate Cancer Cells. *Int J Endocrinol* **2016**, 6437585, doi:10.1155/2016/6437585 (2016).

20 Cook, M. B. *et al.* Relationships between Circulating and Intraprostatic Sex Steroid Hormone Concentrations. *Cancer Epidemiol Biomarkers Prev* **26**, 1660-1666, doi:10.1158/1055-9965.EPI-17-0215 (2017).

21 Bosland, M. C. The role of steroid hormones in prostate carcinogenesis. *J Natl Cancer Inst Monogr*, 39-66, doi:10.1093/oxfordjournals.jncimonographs.a024244 (2000).

22 Sengul, S., Erturk, S., Khan, A. M. & Batuman, V. Receptor-associated protein blocks internalization and cytotoxicity of myeloma light chain in cultured human proximal tubular cells. *PLoS One* **8**, e70276, doi:10.1371/journal.pone.0070276 (2013).

23 Willnow, T. E. *et al.* Defective forebrain development in mice lacking gp330/megalin. *Proc Natl Acad Sci U S A* **93**, 8460-8464, doi:10.1073/pnas.93.16.8460 (1996).

24 Leheste, J. R. *et al.* Megalin knockout mice as an animal model of low molecular weight proteinuria. *Am J Pathol* **155**, 1361-1370, doi:10.1016/S0002-9440(10)65238-8 (1999).

25 Birbach, A., Casanova, E. & Schmid, J. A. A Probasin-MerCreMer BAC allows inducible recombination in the mouse prostate. *Genesis* **47**, 757-764, doi:10.1002/dvg.20558 (2009).

26 Grant, C. E., Bailey, T. L. & Noble, W. S. FIMO: scanning for occurrences of a given motif. *Bioinformatics* **27**, 1017-1018, doi:10.1093/bioinformatics/btr064 (2011).

27 Bhanvadia, R. R. *et al.* MEIS1 and MEIS2 expression and prostate cancer progression: A role for HOXB13 binding partners in metastatic disease. *Clinical Cancer Research* **24**, 3668-3680, doi:10.1158/1078-0432.CCR-17-3673 (2018).

28 Pflueger, D. *et al.* Discovery of non-ETS gene fusions in human prostate cancer using next-generation RNA sequencing. *Genome Res* **21**, 56-67, doi:10.1101/gr.110684.110 (2011).

29 Robinson, D. *et al.* Integrative clinical genomics of advanced prostate cancer. *Cell* **161**, 1215-1228, doi:10.1016/j.cell.2015.05.001 (2015).

30 Zhai, X. Y. *et al.* Cubilin- and megalin-mediated uptake of albumin in cultured proximal tubule cells of opossum kidney. *Kidney Int* **58**, 1523-1533, doi:10.1046/j.1523-1755.2000.00314.x (2000).

31 Rosner, W., Hryb, D. J., Kahn, S. M., Nakhla, A. M. & Romas, N. A. Interactions of sex hormone-binding globulin with target cells. *Mol Cell Endocrinol* **316**, 79-85, doi:10.1016/j.mce.2009.08.009 (2010).

32 Abboud, M. *et al.* 1,25-Dihydroxycholecalciferol (calcitriol) modifies uptake and release of 25-hydroxycholecalciferol in skeletal muscle cells in culture. *J Steroid Biochem Mol Biol* **177**, 109-115, doi:10.1016/j.jsbmb.2017.10.018 (2018).

33 Forrest, K. Y. & Stuhldreher, W. L. Prevalence and correlates of vitamin D deficiency in US adults. *Nutr Res* **31**, 48-54, doi:10.1016/j.nutres.2010.12.001 (2011).

34 Mohler, J. L. *et al.* Racial differences in prostate androgen levels in men with clinically localized prostate cancer. *J Urol* **171**, 2277-2280 (2004).

35 Richard, A. *et al.* Racial variation in sex steroid hormone concentration in black and white men: a meta-analysis. *Andrology* **2**, 428-435, doi:10.1111/j.2047-2927.2014.00206.x (2014).

36 Rowling, M. J., Kemmis, C. M., Taffany, D. A. & Welsh, J. Megalin-mediated endocytosis of vitamin D binding protein correlates with 25-hydroxycholecalciferol actions in human mammary cells. *J Nutr* **136**, 2754-2759 (2006).

37 Howlader N, N. A., Krapcho M, Miller D, Brest A, Yu M, Ruhl J, Tatalovich Z, Mariotto A, Lewis DR, Chen HS, Feuer EJ, Cronin KA. *SEER Cancer Statistics Review, 1975-2016*, <https://seer.cancer.gov/csr/1975_2016/> (2018).

38 Giangreco, A. A. *et al.* Tumor suppressor microRNAs, miR-100 and -125b, are regulated by 1,25-dihydroxyvitamin D in primary prostate cells and in patient tissue. *Cancer prevention research* **6**, 483-494, doi:10.1158/1940-6207.CAPR-12-0253 (2013).

39 Nonn, L., Peng, L., Feldman, D. & Peehl, D. M. Inhibition of p38 by vitamin D reduces interleukin-6 production in normal prostate cells via mitogen-activated protein kinase phosphatase 5: implications for prostate cancer prevention by vitamin D. *Cancer research* **66**, 4516-4524, doi:10.1158/0008-5472.CAN-05-3796 (2006).

40 Kregel, S. *et al.* Acquired resistance to the second-generation androgen receptor antagonist enzalutamide in castration-resistant prostate cancer. *Oncotarget* **7**, doi:10.18632/oncotarget.8456 (2016).

41 Livak, K. J. & Schmittgen, T. D. Analysis of relative gene expression data using real-time quantitative PCR and the 2(-Delta Delta C(T)) Method. *Methods* **25**, 402-408, doi:10.1006/meth.2001.1262 (2001).

42 Higashi, T. *et al.* Determination of prostatic androgens in 10 mg of tissue using liquid chromatography-tandem mass spectrometry with charged derivatization. *Anal Bioanal Chem* **382**, 1035-1043, doi:10.1007/s00216-005-3233-1 (2005).

43 Zang, T. *et al.* Simultaneous quantitation of nine hydroxy-androgens and their conjugates in human serum by stable isotope dilution liquid chromatography electrospray ionization tandem mass spectrometry. *J Steroid Biochem Mol Biol* **165**, 342-355, doi:10.1016/j.jsbmb.2016.08.001 (2017).

44 Maund, S. L., Nolley, R. & Peehl, D. M. Optimization and comprehensive characterization of a faithful tissue culture model of the benign and malignant human prostate. *Lab Invest* **94**, 208-221, doi:10.1038/labinvest.2013.141 (2014).

45 Karthaus, W. R. *et al.* Regenerative potential of prostate luminal cells revealed by single-cell analysis. *Science* **368**, 497-505, doi:10.1126/science.aay0267 (2020).

A.

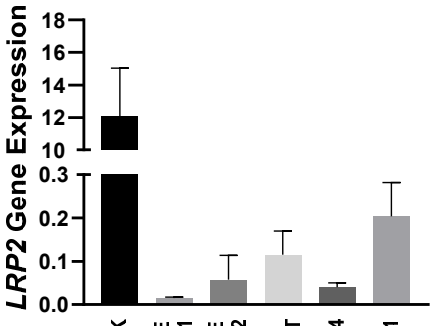

B.

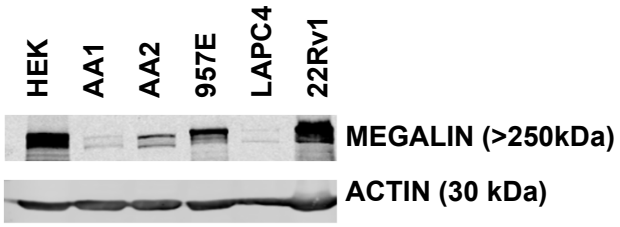

C.

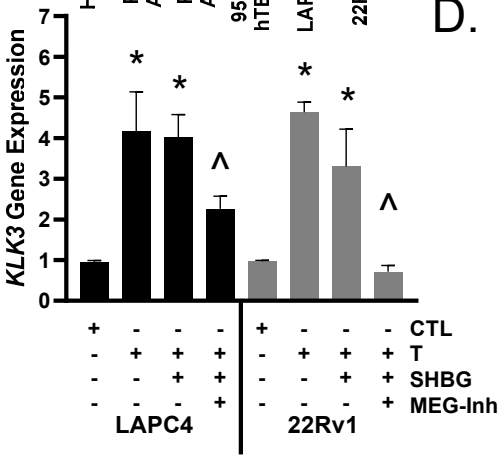

D.

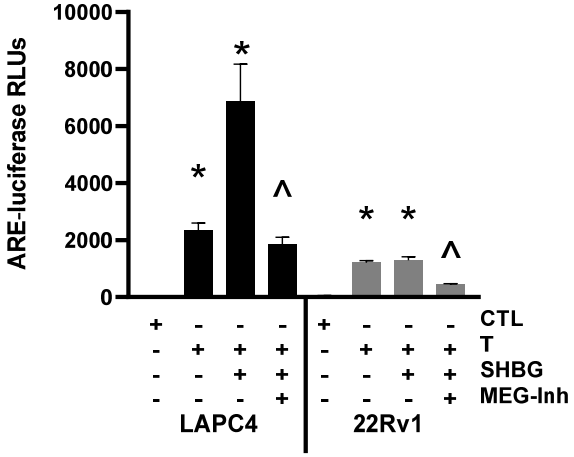

E.

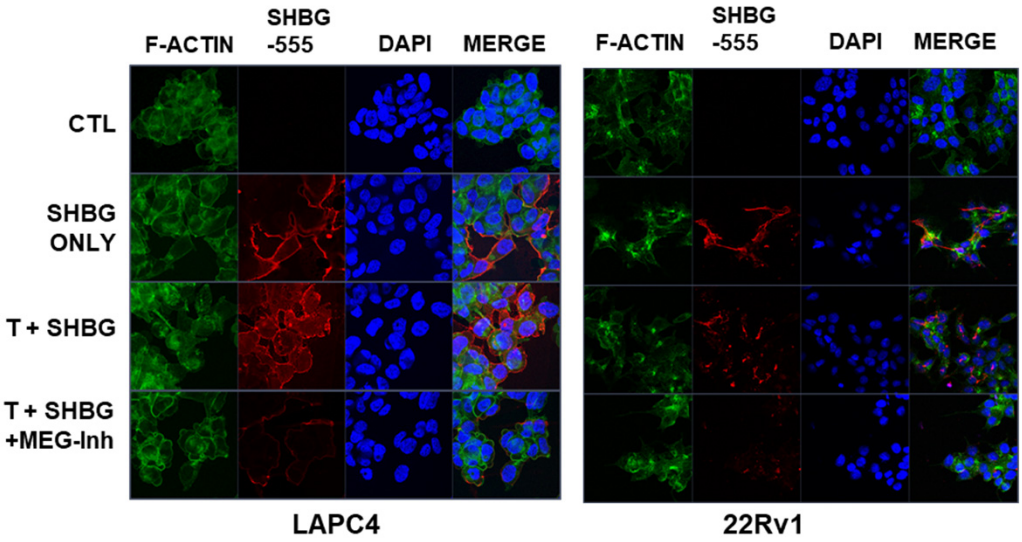

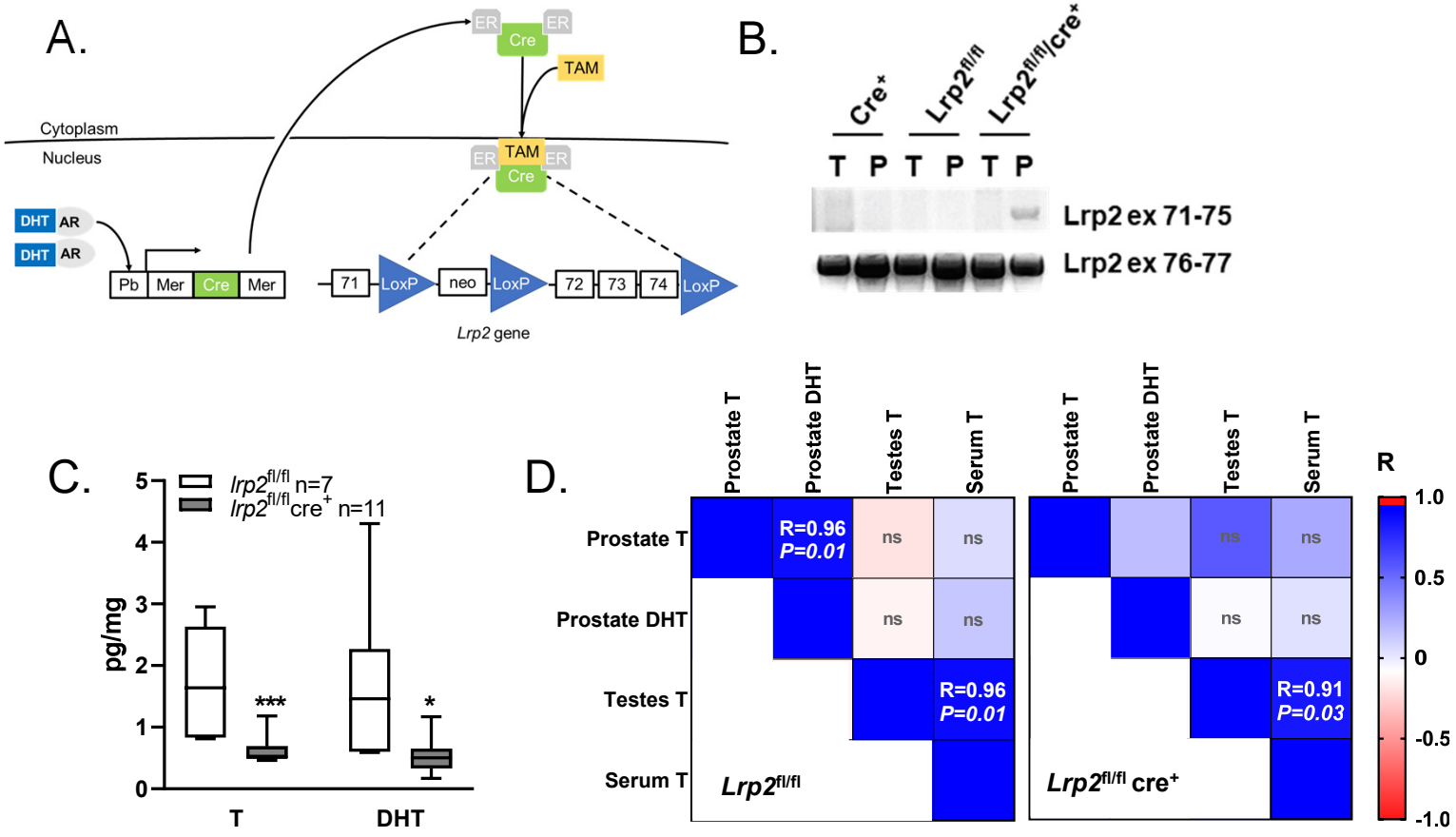

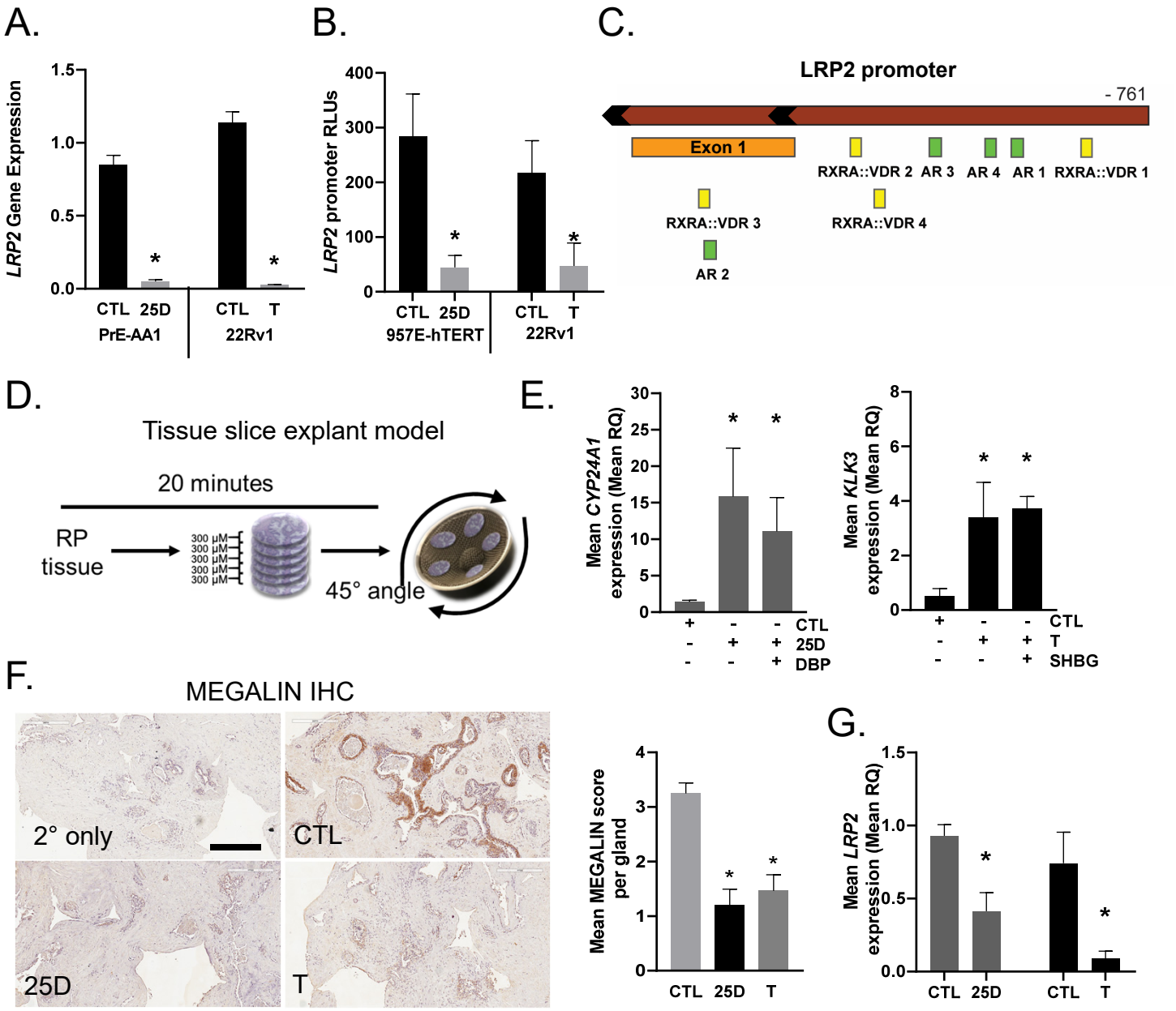

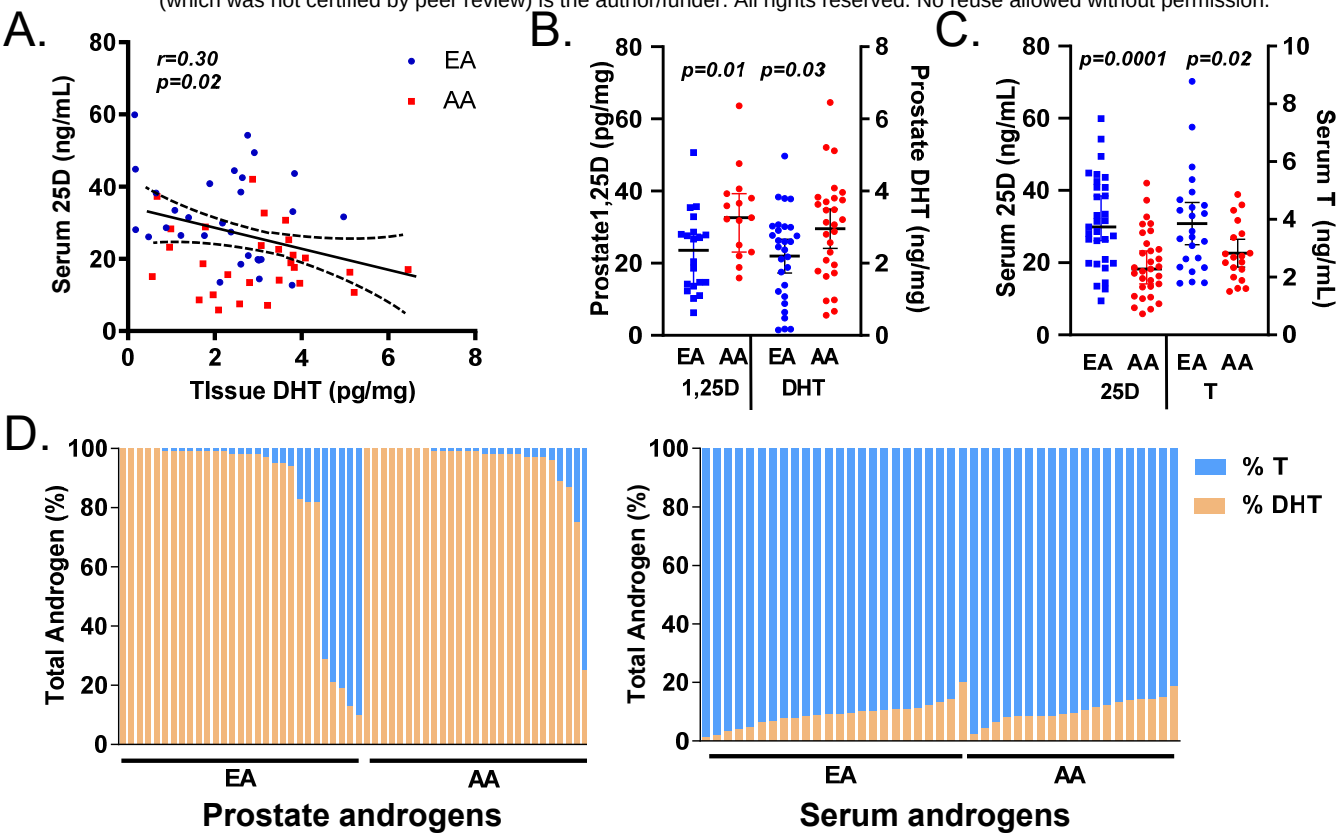

A.

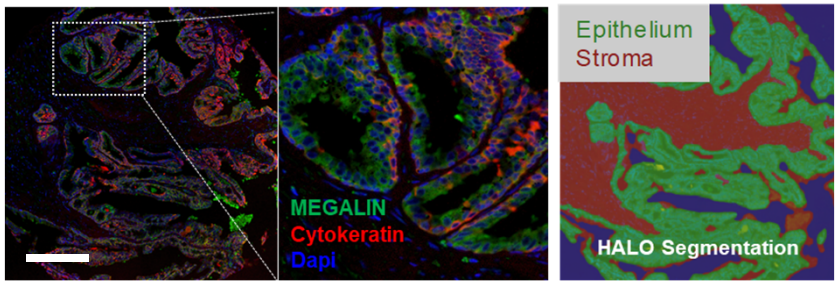

B.

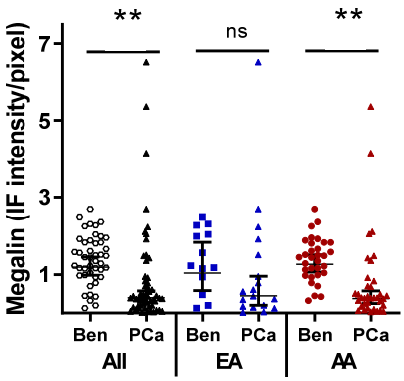

C.

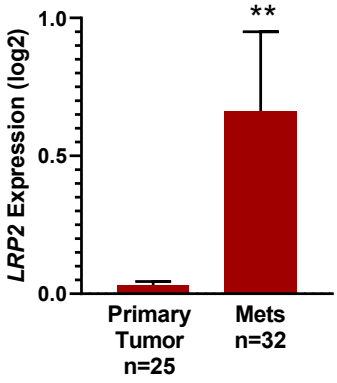

Supplemental Figures

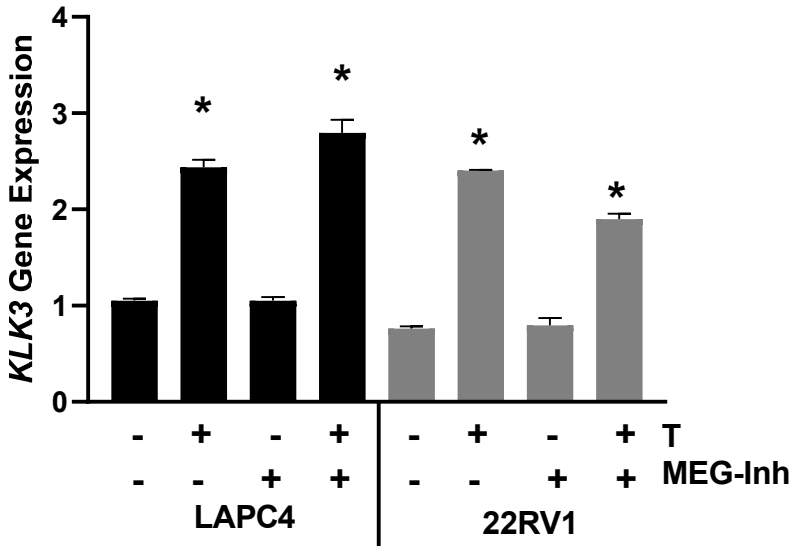

Figure S1. MEGALIN inhibitor does not impact activity and import of T alone. RT-qPCR for *KLK3* following 16 hours of 10 nM T treatment. Cells were pretreated with 1 μM MEG-inhibitor for 1 hour before T. Expression shown as relative quantitation to *HRPT*. Error bars are SEM. *p<0.01

A.

5'CCTGTATCCTATCAGGGGAAACCAAGATATCCGAAGGAGCCTAGAGAGATCAGGCCAGGAATGAAGGT
VDR1
CACAGATCTCCATCCAGCAGGCTCTTTACTCCTTCCCTTCCCTACCCCCGCCTCTTTCCCTTTCTTTCTCT
AR 1 AR 4
TTCCTTCATTTTTACTTGTCTGGTTGTGCTTTCCTTTTCCATTTCTTATTTTTTCTTTCTCTTCTCTATTCTTG
ACTTTCCTCCTCGTCCATTTCTTTCCATTGCTCATTTAGTAAAACTGCGTCCGTGCAGATTTCCCCGTGAG
CCGCCTCGCCGGCTTCACTTAGGAGTGCATGCGCCTGTATGAGTGCGTGTGTCTGTGCGGGGCAAACCC
TGCGGAGAGGCGAGGGCAGCGCGTGTGCACGTGTGAGTGTGCCTGTGAGAGTGTGCGCACAGGAGTGT
GCTCTTGTATGCACGCGTAAAGGGGACTGTGTATGTCGGCGTTGAAGTGTGACTGTGGAATGTGCGCGC
GTGTGTGACTGGCGTGTATGAGTGAATCTGTGTCAGTTGGTGTGAGAGTGTGCACACGCCTGTGTGAGT
AR 3
GTCCCTGTGTGAGCACGCGTGTGTTCGAGTGCCCACTCCTCCCCGCGCTGCAAAGTGCAGGGGGCGGG
VDR4
CCGGGCGGCAGGGGGCCTGCCCGCTGGATTCCCGCATGCTTGTTCCGGGGCGGTCGGGTCTAAAGGG
VDR2
CTTTATGCACTGTCTGGAGGGTGGGGACTGGCGCGGGTAGAAAACGGGATGCCTCGGGCGTGGGGGCA
GGCTTTTGGCCACTAGGAGCTGGCGGAGGTGCAGACCTAAAGGAGCGTTCGCTAGCAGAGGCGCTGCC
GGTGCGGTGTGCTACGCGCGCCCACCTCCCGGGGAAGGAACGGCGAGGCCGGGGACCGTCGCGGAG
AR 2 VDR3
ATGGATCGCGGGCCGGCAGCAGTGGCGTGCACGCTGCTCCTGGCTCTCGTCGCCTGCCTAGCGCCGGC
CAGTGGCCAAGGTAAGAGCCCAGCCAGAG-3'

B.

Motif ID	P-Value	Matched Sequence
RXRA::VDR 1	0.000307	AGGTCACAGATCTCC
RXRA::VDR 2	0.002520	GGGCGGTCGGGTCTA
RXRA::VDR 3	0.006550	CGGTCCCCGGCCTCG
RXRA::VDR 4	0.006940	GCGCTGCAAAGTGCA
AR 1	0.000211	AAGCACAACCAGACA
AR 2	0.000390	AGGAACGGCGAGGCC
AR 3	0.000626	AGGGACACTCACACA
AR 4	0.000778	GAGAAGAGAAAGAAA

Figure S2. Vitamin D receptor and androgen receptor response elements in LRP2 promoter. A, -791 bp of LRP2 promoter showing mapped areas for VDR and AR response elements. **B,** Jasper prediction of the binding sites with P-value. Note that VDR binds VDREs as an obligate heterodimer with RXRα.

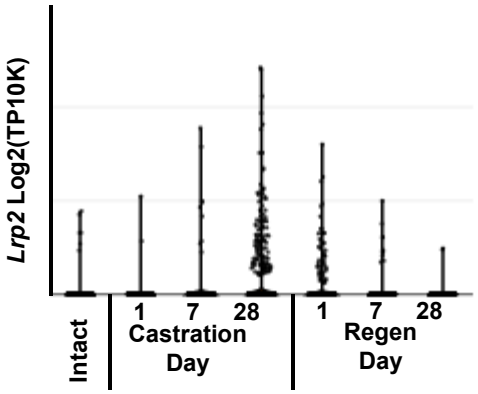

Figure S3. *Lrp2* is regulated by androgens in mouse prostate. scRNAseq data for *Lrp2* expression in mouse prostate epithelial cells following castration and regeneration with testosterone add back. Data from Karthaus et al 2020.

Table S1. Cell and tissue characteristics

MODEL	TISSUE	MORPHOLOGY	DISEASE	ETHINICITY
PrE-AA1	Prostate	Epithelial	Benign	African American
PrE-AA2	Prostate	Epithelial	Benign	African American
957E-hTERT	Prostate	Epithelial	Cancer (local)	Unknown
HEK293	Kidney	Epithelial	Benign	Unknown
LAPC4	Prostate	Epithelial	Cancer (lymph node)	Unknown
TS-AA1	Prostate	Epithelial	Benign	African American
TS-H1	Prostate	Epithelial	Benign	Hispanic

Table S2. Primer sequences

SPECIES	GENE	FORWARD (5' -> 3')	REVERSE (5' -> 3')
HUMAN	***LRP2***	CTCCTGGGTGTGTGACCAA	CATCGGGGCAGTCTCTGAC
	KLK3	TCCAATGACGTGTGTGCGCA	CCTTGATCCACTTCCGGTAA
	CYP24A1	GGCAACAGTTCTGGGTGAAT	ATTTGAGGACAATCCAACA
	CYP27B1	TTTGCATCTCTTCCCTTTGG	CTCAGGCTGCACCTCAAAAT
	VDR	GACCTGTGGCAACCAAGACT	GAACTTGATGAGGGGCTCAA
	SRD5A2	ATATATTGCGCCAGCTCAGG	GGAAATTGGCTCCAGAAACA
	AR	TTGTGTCAAAAGCGAAATGG	CAATGGGCAAAACATGGTC
	RPL13A	GGATAAGAAACCCTGCGACA	CTCGACCATCAAGCACCAG
	HPRT	TGCTGACCTGCTGGATTACA	CTGCATTGTTTTGCCAGTGT
MOUSE	***Pb-MerCreMer*-mutant (genotyping)**	ACGACCAAGTGACAGCAATG	TAAGCAATCCCCAGAAATGC
	***Pb-MerCreMer*-wild type (genotyping)**	CTAGGCCACAGAATTGAAAGATCT	GTAGGTGGAAATTCTAGCATCATC
	***Lrp2-Flox* (genotyping, *wt = 206bp, flox=320bp*)**	CACCATGTCCCTCAGTTGTG	CACCATGTCCCTCAGTTGTG
	***Lrp2* exons 71-75 (recombination)**	CACCGTTGAGTGTGATGCAG	CACCGATGTCCATGTTCACA
	***Lrp2* exons 76-77 (control)**	CTGGTTTTCCACATTTTCTGG	CTGGTTTTCCACATTTTCTGG

Figure 1B

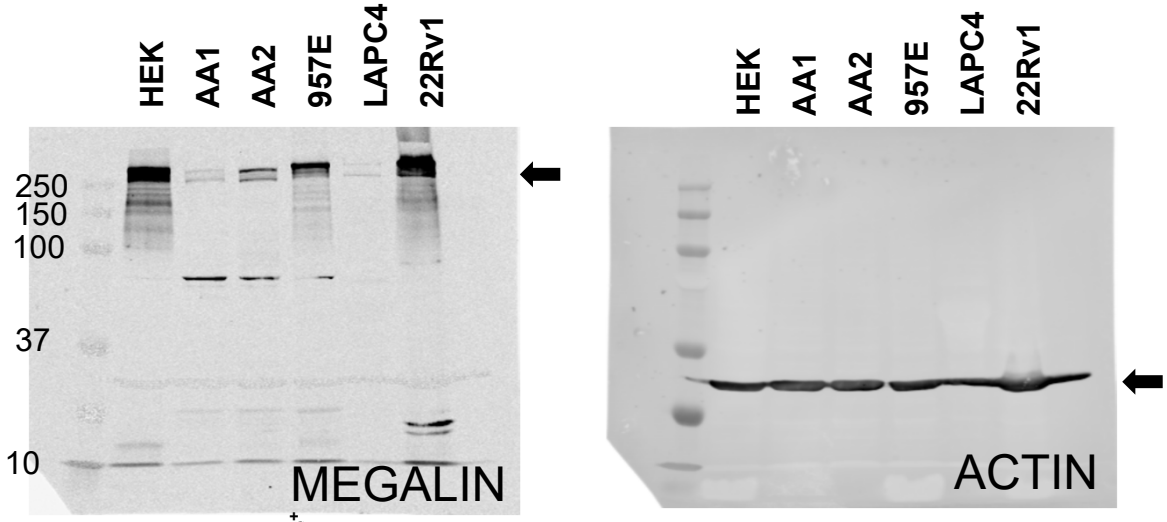

Figure 2B

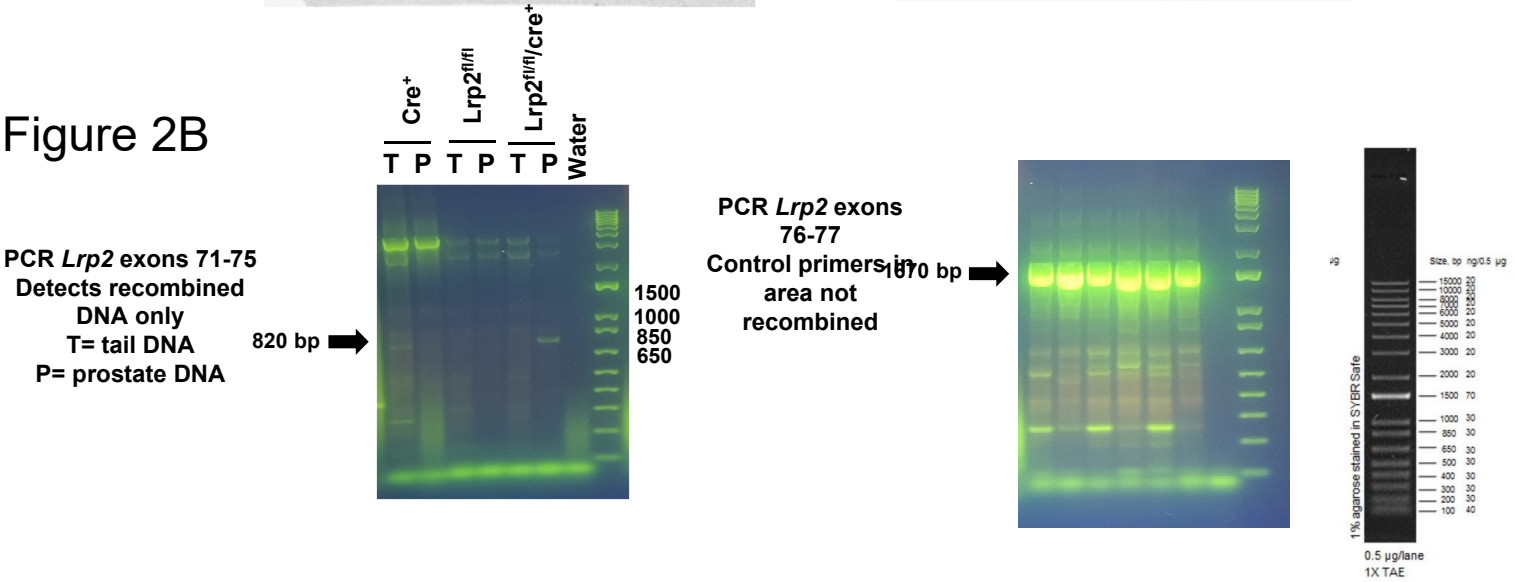

Figure S3

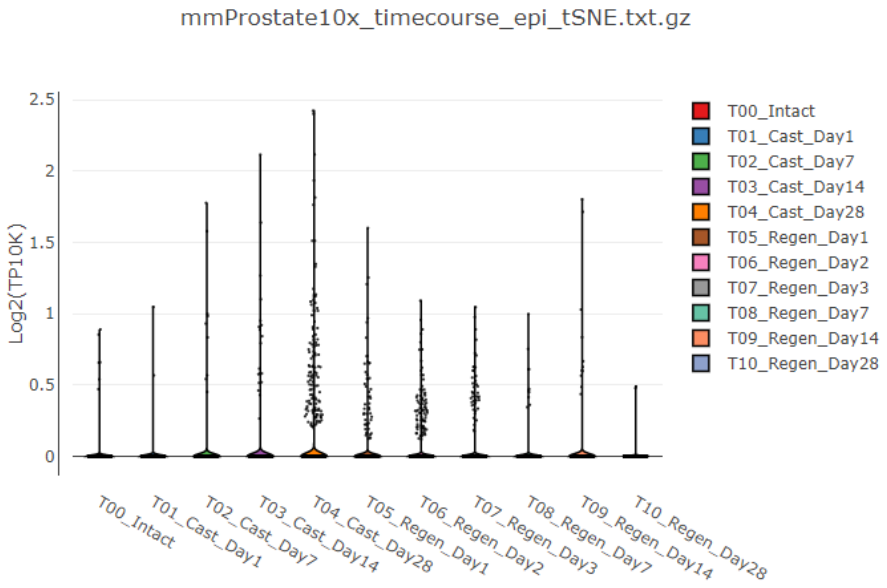

https://singlecell.broadinstitute.org/single_cell/study/SCP859/regenerative-potential-of-prostate-luminal-cells-revealed-by-single-cell-analysis-mouse?genes=Lrp2&cluster=mmProstate10x_timecourse_epi_tSNE.txt.gz&spatialGroups=--&annotation=timepoint--group--study&subsample=all&tab=distribution&distributionPlot=violin&distributionPoints=all#study-visualize